Cooperative Optimization-Based Efficient Autonomous Parameter Design for Cascade Feedback Control System

1st Eitaro Kuroda
Department of Electrical and Mechanical Engineering
Nagoya Institute of Technology
Nagoya, Japan
Email: e.kuroda.963@stn.nitech.ac.jp

2nd Hiroaki Noda
Department of Electrical and Mechanical Engineering
Nagoya Institute of Technology
Nagoya, Japan
Email: h.noda.268@stn.nitech.ac.jp

3rd Yoshihiro Maeda
Department of Electrical and Mechanical Engineering
Nagoya Institute of Technology
Nagoya, Japan
Email: ymaeda@nitech.ac.jp

4th Makoto Iwasaki
Department of Electrical and Mechanical Engineering
Nagoya Institute of Technology
Nagoya, Japan
Email: iwasaki@nitech.ac.jp

***Abstract*—In industrial servo systems, cascade feedback (FB) control systems are widely used for the high-speed and high-accuracy positioning control. In general, since the parameter design for the multiple controllers is a time-consuming task that requires expert skills for designers, development of an autonomous design method based on mathematical optimization becomes a major challenge. In this paper, a cooperative optimization method presented recently for single-loop FB controller design is applied to an example position/velocity cascade controller design for a laboratory piezoelectric-driven fast steering mirror, in comparison with the conventional autonomous design method based on a genetic algorithm (GA). In addition, a practical feasible initial parameter design method in cooperative optimization for the cascade controller design is newly presented to realize the efficient autonomous design.**

***Index Terms*—autonomous design, cascade feedback control system, cooperative optimization, fast steering mirror, sensitivity characteristic**

I. Introduction

One of the major design requirements for the high-speed and high-accuracy positioning control of industrial servo systems is making the feedback (FB) control system less sensitive to disturbance. Cascade systems with an inner loop and outer loop are widely used in industry, and such systems achieve excellent low-sensitivity characteristics [1]–[4]. In addition, as multiple element compensators such as a PID compensator and a notch filter are utilized in the systems, the parameters of the compensators can be more easily tuned by manual than those of an unfixed structure FB controller such as an H_∞ output FB controller [5]. However, the sensitivity characteristics are affected by the characteristics of all control loops; hence, the FB controller parameters of each loop need to be optimized to achieve low sensitivity. In particular, when controlling servo systems with high-order resonant modes, higher-order controller structures require more parameters to robustly stabilize the resonant modes, which involves significant design work for the designer.

To address this issue, autonomous parameter design methods based on mathematical optimization have been proposed to reduce the design work. These methods are categorized into two main types: iterative and metaheuristic methods. A design method based on an iterative method is outlined in [6], which proposes an autonomous design method for a P-PI cascade control system with a notch filter based on a non-smooth optimization method [7]. By formulating the problem to optimize all FB controller parameters at once, this method enables parameter design that maximizes frequency bands with low sensitivity. However, the optimization problem is a non-convex problem, and the initial parameters (initial point) in the solution need to be adjusted by trial and error to obtain the required sensitivity characteristics, which is generally difficult. Meanwhile, metaheuristic-based design methods that do not require the precise setting of initial point have been proposed. For example, [8]–[10] propose autonomous parameter design methods based on genetic algorithms (GA) and neural networks. However, in general, there are concerns that design times will increase when the system involves a large number of design parameters. Therefore, improved efficient optimization methods for cascade control systems are greatly desired.

In [11], a cooperative optimization method combining iterative sequential quadratic programming (SQP) and a metaheuristic GA has been presented to autonomously design a single-loop FB control system. The cooperative optimization method provides the fast and efficient optimization for FB controller parameters by combining SQP and GA; however, its effectiveness in a cascade control system has not yet been confirmed. In this study, we will formulate the optimization problem of FB controller parameters in a cascade control

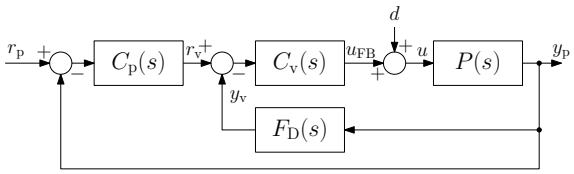

Fig. 1. Block diagram of cascade control system.

system for the cooperative optimization, and newly derive a practical feasible initial point condition to realize the efficient cascade controller design. The cooperative optimization method is applied to an example autonomous design problem of a position/velocity cascade control system for a laboratory piezoelectric-driven fast steering mirror (FSM). The effectiveness of the cooperative optimization method is verified by comparing the design efficiency with that of a conventional GA-based design method.

II. Design Problem of a Cascade Control System

In this study, we will consider the position/velocity cascade control system shown in Fig. 1. Here, $P(s)$: plant (FSM), $C_\mathrm{p}(s)$: P controller for position control, $C_\mathrm{v}(s)$: PI controller and notch filter for velocity control, $F_\mathrm{D}(s)$: an approximate differentiator, r_p: position command, r_v: velocity command, y_p: position, y_v: velocity, u_FB: FB control input, u: control input, d: disturbance. $C_\mathrm{p}(s)$, $C_\mathrm{v}(s)$, and $F_\mathrm{D}(s)$ can be expressed by the following equations.

$$C_\mathrm{p}(s) = K_\mathrm{pp} \tag{1}$$

$$C_\mathrm{v}(s) = \left(K_\mathrm{vp} + \frac{K_\mathrm{vi}}{s}\right)\prod_{i=1}^{N_\mathrm{v}} \frac{s^2 + 2\zeta_{\mathrm{vn}i}\omega_{\mathrm{v}i}s + \omega_{\mathrm{v}i}^2}{s^2 + 2\zeta_{\mathrm{vd}i}\omega_{\mathrm{v}i}s + \omega_{\mathrm{v}i}^2} \tag{2}$$

$$F_\mathrm{D}(s) = \frac{s}{\frac{1}{\omega_\mathrm{D}}s + 1} \tag{3}$$

In the equations above, K_pp and K_vp: proportional gains, K_vi: integral gain, N_v: the number of stages of notch filter, $\zeta_{\mathrm{vn}i}$ and $\zeta_{\mathrm{vd}i}$: damping coefficients, $\omega_{\mathrm{v}i}$: center frequency, and ω_D: the cutoff frequency of low-pass filter for approximate differentiation. The purpose of the notch filter in $C_\mathrm{v}(s)$ is to stabilize the resonance mode of $P(s)$ using the gain/phase stabilization method [6], which allows $C_\mathrm{p}(s)$ and $C_\mathrm{v}(s)$ to have higher gains.

The design problem in this study is to enable autonomous design to set all the parameters of $C_\mathrm{p}(s)$, $C_\mathrm{v}(s)$, and $F_\mathrm{D}(s)$ in (4) such that they satisfy the desired stability margin for $P(s)$ (gain margin g_m [dB] and phase margin ϕ_m [deg]), as well as maximize the band with low sensitivity to disturbance d.

$$\boldsymbol{\rho} = [K_\mathrm{pp}\ K_\mathrm{vp}\ K_\mathrm{vi}\ \zeta_{\mathrm{vn}i}\ \zeta_{\mathrm{vd}i}\ \omega_{\mathrm{v}i}\ \omega_\mathrm{D}],\quad i = 1, \cdots, N_\mathrm{v} \tag{4}$$

III. GA-based Autonomous Parameter Design Method

In this section, we define the method of optimizing the parameters $\boldsymbol{\rho}$ in (4) using a GA.

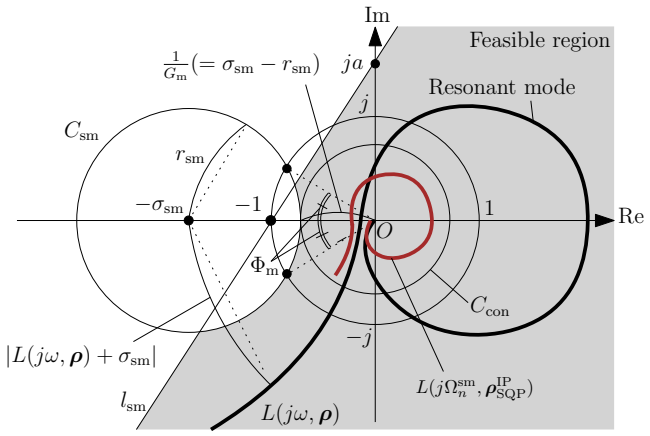

Fig. 2. Stability constraint for Nyquist trajectory.

A. Objective function considering expansion of low-sensitivity band

We formulate an objective function, considering the need to bring the actual sensitivity characteristic $S(j\omega)\left(=\frac{u(j\omega)}{d(j\omega)}\right)$ of the cascade control system closer to the ideal sensitivity characteristic $S_\mathrm{ds}(j\omega)$ [3], [11]. The following equation shows the actual sensitivity characteristic $S(j\omega)$ of the cascade control system in Fig. 1.

$$S(j\omega) = \frac{u(j\omega)}{d(j\omega)} = \frac{1}{1 + L(j\omega,\boldsymbol{\rho})} \tag{5}$$

$$L(j\omega,\boldsymbol{\rho}) = (C_\mathrm{p}(j\omega) + F_\mathrm{D}(j\omega))C_\mathrm{v}(j\omega)P(j\omega) \tag{6}$$

In (5), $L(j\omega,\boldsymbol{\rho})$ is the actual open-loop characteristic of the cascade control system. We then define the ideal open-loop characteristic $L_\mathrm{ds}(j\omega)$ in (7) from $S_\mathrm{ds}(j\omega)$ and evaluate the objective function $J_\mathrm{obj}(\boldsymbol{\rho})$ representing the distance between the actual open-loop characteristics $L(j\omega,\boldsymbol{\rho})$ and $L_\mathrm{ds}(j\omega)$ in (8). $\Omega_m^\mathrm{obj}(m = 1, \cdots, N_\mathrm{obj})$ is the discrete frequency for evaluation.

$$L_\mathrm{ds}(j\omega) = \frac{1 - S_\mathrm{ds}(j\omega)}{S_\mathrm{ds}(j\omega)} \tag{7}$$

$$J_\mathrm{obj}(\boldsymbol{\rho}) = \sum_{m=1}^{N_\mathrm{obj}} \left|L_\mathrm{ds}(j\Omega_m^\mathrm{obj}) - L(j\Omega_m^\mathrm{obj},\boldsymbol{\rho})\right| \tag{8}$$

B. Stability constraints on the cascade control system

Fig. 2 shows a Nyquist trajectory of the open-loop characteristic $L(j\omega,\boldsymbol{\rho})$. In this figure, the circle C_sm with its center at $(-\sigma_\mathrm{sm},\ j0)$ and radius r_sm define the stability margin. The point where C_sm intersects with the real axis corresponds to the gain margin $g_\mathrm{m}(=20\log_{10}G_\mathrm{m})$ [dB]. The points where C_sm intersects with the unit circle centered at the origin correspond to the phase margin $\phi_\mathrm{m}(=180\Phi_\mathrm{m}/\pi)$ [deg]. l_sm is a straight line passing through $(-1,\ j0)$ at angle a.

The stability margins are ensured by making the Nyquist trajectory $L(j\Omega_n^\mathrm{sm},\boldsymbol{\rho})$ at the discrete frequency Ω_n^sm pass

through the region outside $C_{\rm sm}$ [12] and to the right side of $l_{\rm sm}$, expressed by the following stability constraints.

$$h_{C\rm sm}(\Omega_n^{\rm sm},\boldsymbol{\rho}) = |L(j\Omega_n^{\rm sm},\boldsymbol{\rho})+\sigma_{\rm sm}|^2 - r_{\rm sm}^2 \geq 0 \quad (9)$$

$$h_{l\rm sm}(\Omega_n^{\rm sm},\boldsymbol{\rho}) = a\left(\mathrm{Re}\left[L(j\Omega_n^{\rm sm},\boldsymbol{\rho})\right]+1\right) - \mathrm{Im}\left[L(j\Omega_n^{\rm sm},\boldsymbol{\rho})\right] \geq 0 \quad (10)$$

Note that the line $l_{\rm sm}$ is a constraint that prevents the Nyquist trajectory $L(j\Omega_n^{\rm sm},\boldsymbol{\rho})$ at low frequencies from passing through the upper part of $C_{\rm sm}$ in the second quadrant.

C. Optimization problem

The optimization problem of parameter $\boldsymbol{\rho}$ by the GA is represented as follows, considering (8)–(10).

$$\min_{\boldsymbol{\rho}} \quad J_{\rm obj}(\boldsymbol{\rho}) + \sum_{n=1}^{N_{\rm sm}} \left\{J_{C\rm sm}(\Omega_n^{\rm sm},\boldsymbol{\rho}) + J_{l\rm sm}(\Omega_n^{\rm sm},\boldsymbol{\rho})\right\} \quad (11)$$

$$J_{C\rm sm}(\Omega_n^{\rm sm},\boldsymbol{\rho}) = \begin{cases} W_{C\rm sm} & (h_{C\rm sm}(\Omega_n^{\rm sm},\boldsymbol{\rho})<0) \\ 0 & (h_{C\rm sm}(\Omega_n^{\rm sm},\boldsymbol{\rho})\geq 0) \end{cases} \quad (12)$$

$$J_{l\rm sm}(\Omega_n^{\rm sm},\boldsymbol{\rho}) = \begin{cases} W_{l\rm sm} & (h_{l\rm sm}(\Omega_n^{\rm sm},\boldsymbol{\rho})<0) \\ 0 & (h_{l\rm sm}(\Omega_n^{\rm sm},\boldsymbol{\rho})\geq 0) \end{cases} \quad (13)$$

In (11), $J_{C\rm sm}(\Omega_n^{\rm sm},\boldsymbol{\rho})$ and $J_{l\rm sm}(\Omega_n^{\rm sm},\boldsymbol{\rho})$ are penalty terms for the constraints in (9) and (10), respectively. $W_{C\rm sm}$ and $W_{l\rm sm}$ are weight values. Penalties are imposed on $N_{\rm sm}$-point discrete frequencies. The GA method can search for the values of $\boldsymbol{\rho}$ that maximize the low-sensitivity band while maintaining stability. However, (11) is a non-convex optimization problem; hence, there are concerns that design will take longer when there are a large number of parameters.

IV. Cooperative optimization-based autonomous parameter design method

A. Autonomous design algorithm

Fig. 3 shows a flowchart of the autonomous parameter design algorithm. In this chart, $\boldsymbol{\rho}_{\rm SQP}$ is a PI parameter vector and $C_{\rm v}(s)$ can be expressed using $\boldsymbol{\rho}_{\rm SQP}$ as follows.

$$C_{\rm v}(s) = \boldsymbol{\Psi}_{\rm GA}^{\rm v}(s)\boldsymbol{\rho}_{\rm SQP}^{\top} \quad (14)$$

$$\boldsymbol{\Psi}_{\rm GA}^{\rm v}(s) = \begin{bmatrix} 1 & \frac{1}{s} \end{bmatrix} \prod_{i=1}^{N_{\rm v}} \frac{s^2+2\zeta_{{\rm vn}i}\omega_{{\rm v}i}s+\omega_{{\rm v}i}^2}{s^2+2\zeta_{{\rm vd}i}\omega_{{\rm v}i}s+\omega_{{\rm v}i}^2} \quad (15)$$

$$\boldsymbol{\rho}_{\rm SQP} = \begin{bmatrix} K_{\rm vp} & K_{\rm vi} \end{bmatrix} \in \mathbb{R}^{1\times 2} \quad (16)$$

$\boldsymbol{\rho}_{\rm GA}$ is a vector of the parameters other than $\boldsymbol{\rho}_{\rm SQP}$ and is defined by the following equation.

$$\boldsymbol{\rho}_{\rm GA} = \Big[K_{\rm pp}\ \zeta_{{\rm vn}i}\ \zeta_{{\rm vd}i}\ \omega_{{\rm v}i}\ \omega_{\rm D}\Big], i = 1,\cdots,N_{\rm v} \quad (17)$$

Based on [12], $\boldsymbol{\rho}_{\rm SQP}$ and $\boldsymbol{\rho}_{\rm GA}$ are designed via cooperative optimization using SQP and GA, respectively. The procedure of the design algorithm is as follows.

Step 1 Initialize the counter α to $\alpha := 1$ as the number of generations of GA, and randomly generate $N_{\rm ind}$ individuals as the initial population of $\boldsymbol{\rho}_{\rm GA}$.

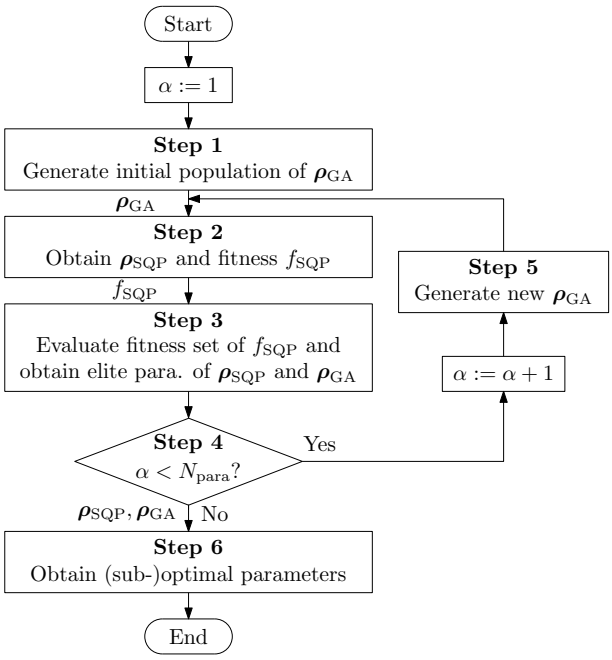

Fig. 3. Flowchart of autonomous FB controller design method.

Step 2 Use SQP to solve the constrained optimization problem of $\boldsymbol{\rho}_{\rm SQP}$ for $\boldsymbol{\rho}_{\rm GA}$ of $N_{\rm ind}$ individuals and determine the fitness value $f_{\rm SQP}$ for $N_{\rm ind}$ individuals. SQP performs optimization from a fixed initial point $\boldsymbol{\rho}_{\rm SQP}^{\rm IP}$.

Step 3 Use GA to compare $N_{\rm ind}$ fitness values $f_{\rm SQP}$ obtained in Step 2 to obtain the elite parameters of $\boldsymbol{\rho}_{\rm SQP}$ and $\boldsymbol{\rho}_{\rm GA}$.

Step 4 If the GA optimization count α exceeds $N_{\rm para}$, end the search and go to Step 6. Otherwise, set $\alpha := \alpha+1$ and go to Step 5 to perform parameter search again.

Step 5 Perform tournament selection, single-point crossover, and genetic operation of mutation to generate a new population of $\boldsymbol{\rho}_{\rm GA}$, then go to Step 2.

Step 6 Obtain the elite parameters of $\boldsymbol{\rho}_{\rm SQP}$ and $\boldsymbol{\rho}_{\rm GA}$ in the $N_{\rm para}$-th generation as the best FB control parameters.

B. Optimization problem of SQP

In this section, we discuss the optimization problem solved by SQP in Step 2 of Fig. 3. First, reformulate (8) by (18) as the objective function of $\boldsymbol{\rho}_{\rm SQP}$.

$$J_{\rm obj}(\boldsymbol{\rho}_{\rm SQP}) \quad = \quad \sum_{m=1}^{N_{\rm obj}} \sqrt{\left[1\ \boldsymbol{\rho}_{\rm SQP}\right]\boldsymbol{Q}_{\rm o}^{m}\left[1\ \boldsymbol{\rho}_{\rm SQP}\right]^{\top}} \quad (18)$$

In (18), $\boldsymbol{Q}_{\mathrm{o}}^{m}$ is defined by the following equations.

$$\begin{aligned}\boldsymbol{Q}_{\mathrm{o}}^{m} &= \mathrm{Re}\left[\boldsymbol{Y}_{\mathrm{o}}^{\top}(j\Omega_m^{\mathrm{obj}})\right]\mathrm{Re}\left[\boldsymbol{Y}_{\mathrm{o}}(j\Omega_m^{\mathrm{obj}})\right] \\ &\quad + \mathrm{Im}\left[\boldsymbol{Y}_{\mathrm{o}}^{\top}(j\Omega_m^{\mathrm{obj}})\right]\mathrm{Im}\left[\boldsymbol{Y}_{\mathrm{o}}(j\Omega_m^{\mathrm{obj}})\right] \in \mathbb{R}^{3\times 3} \quad (19)\\ \boldsymbol{Y}_{\mathrm{o}}(j\Omega_m^{\mathrm{obj}}) &= \left[L_{\mathrm{ds}}(j\Omega_m^{\mathrm{obj}})\right. \\ &\quad \left. -P(j\Omega_m^{\mathrm{obj}})\boldsymbol{\Psi}_{\mathrm{GA}}(j\Omega_m^{\mathrm{obj}})\right] \in \mathbb{C}^{1\times 3} \quad (20)\\ \boldsymbol{\Psi}_{\mathrm{GA}}(j\Omega_m^{\mathrm{obj}}) &= \boldsymbol{\Psi}_{\mathrm{GA}}^{\mathrm{v}}(j\Omega_m^{\mathrm{obj}})\left(C_{\mathrm{p}}(j\Omega_m^{\mathrm{obj}})\right. \\ &\quad \left. +F_{\mathrm{D}}(j\Omega_m^{\mathrm{obj}})\right) \in \mathbb{C}^{1\times 2} \quad (21)\end{aligned}$$

Subsequently, reformulate (9) as a constraint of $\boldsymbol{\rho}_{\mathrm{SQP}}$ as

$$\begin{aligned}&h_{C\mathrm{sm}}(\Omega_n^{\mathrm{sm}}, \boldsymbol{\rho}_{\mathrm{SQP}}) \\ &\quad = [1\ \boldsymbol{\rho}_{\mathrm{SQP}}]\,\boldsymbol{Q}_{\mathrm{sm}}^{n}\,[1\ \boldsymbol{\rho}_{\mathrm{SQP}}]^{\top} - r_{\mathrm{sm}}^2 \geq 0. \quad (22)\end{aligned}$$

$\boldsymbol{Q}_{\mathrm{sm}}^{n}$ in (22) is defined by the following equations.

$$\begin{aligned}\boldsymbol{Q}_{\mathrm{sm}}^{n} &= \mathrm{Re}\left[\boldsymbol{Y}_{\mathrm{sm}}^{\top}(j\Omega_n^{\mathrm{sm}})\right]\mathrm{Re}\left[\boldsymbol{Y}_{\mathrm{sm}}(j\Omega_n^{\mathrm{sm}})\right] \\ &\quad + \mathrm{Im}\left[\boldsymbol{Y}_{\mathrm{sm}}^{\top}(j\Omega_n^{\mathrm{sm}})\right]\mathrm{Im}\left[\boldsymbol{Y}_{\mathrm{sm}}(j\Omega_n^{\mathrm{sm}})\right] \in \mathbb{R}^{3\times 3} \quad (23)\\ \boldsymbol{Y}_{\mathrm{sm}}(j\Omega_n^{\mathrm{sm}}) &= [\sigma_{\mathrm{sm}} \\ &\quad P(j\Omega_n^{\mathrm{sm}})\boldsymbol{\Psi}_{\mathrm{GA}}(j\Omega_n^{\mathrm{sm}})] \in \mathbb{C}^{1\times 3} \quad (24)\\ \boldsymbol{\Psi}_{\mathrm{GA}}(j\Omega_n^{\mathrm{sm}}) &= \boldsymbol{\Psi}_{\mathrm{GA}}^{\mathrm{v}}(j\Omega_n^{\mathrm{sm}})\,(C_{\mathrm{p}}(j\Omega_n^{\mathrm{sm}}) \\ &\quad +F_{\mathrm{D}}(j\Omega_n^{\mathrm{sm}})) \in \mathbb{C}^{1\times 2} \quad (25)\end{aligned}$$

For more details on equations (18) and (22), see [12]. From (18) and (22), the parameter optimization problem of $\boldsymbol{\rho}_{\mathrm{SQP}}$ is expressed by (26). Using SQP, we can obtain the value of $\boldsymbol{\rho}_{\mathrm{SQP}}$ that achieves low sensitivity and also ensures the desired stability margin.

$$\begin{aligned}&\min_{\boldsymbol{\rho}_{\mathrm{SQP}}} \quad J_{\mathrm{obj}}(\boldsymbol{\rho}_{\mathrm{SQP}}) \\ &\text{subject to } h_{C\mathrm{sm}}(\Omega_n^{\mathrm{sm}}, \boldsymbol{\rho}_{\mathrm{SQP}}) \geq 0, \\ &\qquad\qquad n = 1, \cdots, N_{\mathrm{sm}} \quad (26)\end{aligned}$$

Here, let the fitness value f_{SQP} be the minimum value of the constrained optimization problem in (26).

C. Initial point setting

The optimization problem of (26) is defined depending on $\boldsymbol{\rho}_{\mathrm{GA}}$, setting a feasible initial point for $\boldsymbol{\rho}_{\mathrm{SQP}}$ regardless of $\boldsymbol{\rho}_{\mathrm{GA}}$ is necessary for avoiding to stuck the optimization [12]. Therefore, a practical initial point condition for the cascade control system is derived to realize the efficient autonomous design. Because deriving a condition that satisfies (22) for all parameters is difficult, we define the initial point $\boldsymbol{\rho}_{\mathrm{SQP}}^{\mathrm{IP}}$ as $\boldsymbol{\rho}_{\mathrm{SQP}}^{\mathrm{IP}} = \left[0\ K_{\mathrm{vi}}^{\mathrm{IP}}\right]$ and set $K_{\mathrm{vi}}^{\mathrm{IP}}(>0)$ such that $\boldsymbol{\rho}_{\mathrm{SQP}}^{\mathrm{IP}}$ becomes feasible for any $\boldsymbol{\rho}_{\mathrm{GA}}$ generated by the GA. To clarify the sufficient condition of $K_{\mathrm{vi}}^{\mathrm{IP}}$ for (22), the conceptual Nyquist diagram is shown in Fig. 2, where C_{con} is the circle with radius $\sigma_{\mathrm{sm}} - r_{\mathrm{sm}}$ centered on the origin and tangent to C_{sm}. The sufficient condition is the Nyquist trajectory $L(j\Omega_n^{\mathrm{sm}}, \boldsymbol{\rho}_{\mathrm{SQP}}^{\mathrm{IP}})$ being described in C_{con} as follows.

$$\left|L(j\Omega_n^{\mathrm{sm}}, \boldsymbol{\rho}_{\mathrm{SQP}}^{\mathrm{IP}})\right| \leq \sigma_{\mathrm{sm}} - r_{\mathrm{sm}},\ n = 1, \cdots, N_{\mathrm{sm}} \quad (27)$$

By using (6), the left term of (27) satisfies the following inequality, considering that the gains of notch filters are below unit at all Ω_n^{sm}. In (28), $\underline{*}$ is defined as a lower bound and $\overline{*}$ is defined as a upper bound.

$$\begin{aligned}&\left|L(j\Omega_n^{\mathrm{sm}}, \boldsymbol{\rho}_{\mathrm{SQP}}^{\mathrm{IP}})\right| \\ &\leq \left|K_{\mathrm{pp}} + \frac{j\Omega_n^{\mathrm{sm}}}{j\frac{\Omega_n^{\mathrm{sm}}}{\omega_{\mathrm{D}}} + 1}\right| \left|\frac{K_{\mathrm{vi}}^{\mathrm{IP}}}{j\Omega_n^{\mathrm{sm}}}\right| |P(j\Omega_n^{\mathrm{sm}})| \\ &< \sqrt{\frac{\left(\frac{\overline{K_{\mathrm{pp}}}}{\underline{\omega_{\mathrm{D}}}} + 1\right)^2 \overline{\Omega_n^{\mathrm{sm}}}^2 + \overline{K_{\mathrm{pp}}}^2}{\left(\frac{\Omega_n^{\mathrm{sm}}}{\overline{\omega_{\mathrm{D}}}}\right)^2 + 1}} \cdot \frac{K_{\mathrm{vi}}^{\mathrm{IP}}}{\underline{\Omega_n^{\mathrm{sm}}}} \\ &\qquad \cdot \max_n |P(j\Omega_n^{\mathrm{sm}})| \quad (28)\end{aligned}$$

Therefore, the condition for $K_{\mathrm{vi}}^{\mathrm{IP}}$ is derived by (29) and (30).

$$0 < K_{\mathrm{vi}}^{\mathrm{IP}} \leq \kappa \quad (29)$$

$$\kappa = \frac{(\sigma_{\mathrm{sm}} - r_{\mathrm{sm}})\,\underline{\Omega_n^{\mathrm{sm}}}}{\max_n |P(j\Omega_n^{\mathrm{sm}})|} \sqrt{\frac{\left(\frac{\Omega_n^{\mathrm{sm}}}{\overline{\omega_{\mathrm{D}}}}\right)^2 + 1}{\left(\frac{\overline{K_{\mathrm{pp}}}}{\underline{\omega_{\mathrm{D}}}} + 1\right)^2 \overline{\Omega_n^{\mathrm{sm}}}^2 + \overline{K_{\mathrm{pp}}}^2}} \quad (30)$$

D. Optimization problem of GA

In this section, we discuss the optimization problem solved using the GA in Step 3 of Fig. 3. The N_{ind} fitness values f_{SQP} obtained in Step 2 are treated as the fitness values, and the GA obtains the elite parameters of $\boldsymbol{\rho}_{\mathrm{GA}}$ based on the following optimization problem.

$$\min_{\boldsymbol{\rho}_{\mathrm{GA}}} \left\{f_{\mathrm{SQP}}^{(1)}, f_{\mathrm{SQP}}^{(2)}, \cdots, f_{\mathrm{SQP}}^{(N_{\mathrm{ind}}-1)}, f_{\mathrm{SQP}}^{(N_{\mathrm{ind}})}\right\} \quad (31)$$

The penalty term from (13) is applied to f_{SQP} in (31) to consider the constraint in (10), which is expressed as

$$f_{\mathrm{SQP}} := f_{\mathrm{SQP}} + \sum_{n=1}^{N_{\mathrm{sm}}} J_{l\mathrm{sm}}(\Omega_n^{\mathrm{sm}}, \boldsymbol{\rho}_{\mathrm{SQP}}, \boldsymbol{\rho}_{\mathrm{GA}}) \quad (32)$$

$J_{l\mathrm{sm}}$ in (32) is calculated from $\boldsymbol{\rho}_{\mathrm{SQP}}$ and $\boldsymbol{\rho}_{\mathrm{GA}}$. In parameter design using the cooperative optimization method, $\boldsymbol{\rho}_{\mathrm{SQP}}$ and $\boldsymbol{\rho}_{\mathrm{GA}}$ are optimized using SQP and GA, respectively. Note that even if the autonomous design is performed, there is no guarantee that the frequency of the notch filter will become the resonance frequency.

V. Simulation evaluation

A. Piezoelectric-driven fast steering mirror (FSM)

Fig. 4 shows the appearance of the laboratory FSM used as the object of control. The test setup comprises a mirror for reflecting a laser and a tilt stage driven by the piezoelectric actuator (PI, S-331.5SL), and the mirror is fixed to the tilt stage. The mirror tilt angle $\theta_{\mathrm{s}}(s)$ detected by the built-in strain gauge sensors via the amplifier (PI, E-505.10) and is fed back to the servo control system (dSPACE, MicroLabBox). The voltage for the piezoelectric actuator is controlled by the amplifier according to the voltage command $V_{\mathrm{ref}}(= u_{\mathrm{FB}})$ calculated in the servo control system.

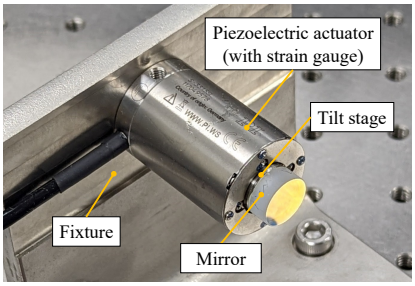

Fig. 4. Exterior of the laboratory FSM.

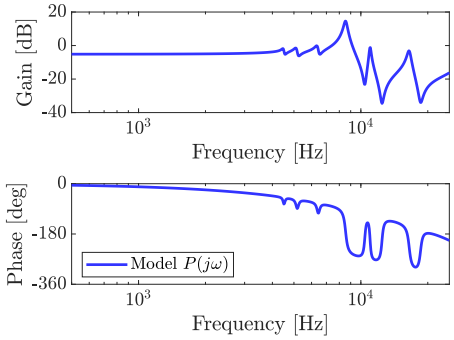

Fig. 5. Frequency characteristics of the plant model.

The mathematical model $P(s) = \theta_{\rm s}(s)/V_{\rm ref}(s)$ from the piezoelectric actuator voltage command to the mirror angle $\theta_{\rm s}(= y_{\rm p})$ is defined by the following equation.

$$P(s) = e^{-T_{\rm D}s} \frac{K_{\rm g}\omega_{\rm amp}}{s+\omega_{\rm amp}} \sum_{\kappa=1}^{7} \frac{k_\kappa}{s^2 + 2\zeta_\kappa\omega_\kappa s + \omega_\kappa^2} \tag{33}$$

Here, $K_{\rm g}$: steady-state gain, including the voltage amplifier, FSM, and sensor, $\omega_{\rm amp}$: cutoff frequency of voltage amplifier, ω_κ: mode resonance frequency, ζ_κ: modal damping coefficient, k_κ: modal gain, and $T_{\rm D}$: equivalent dead time.

Fig. 5 shows the frequency characteristics of the plant model $P(j\omega)$ in (33). The FSM is a mechanical system that has multiple resonance modes and the main resonance is at $2\pi \times 8540$ rad/s.

B. Design specifications

The positioning performance of the FSM is adversely affected by the nonlinear characteristics of hysteresis and creep. To mitigate these effects, the FB control system is required to have low sensitivity in the low-frequency band. In this study, we reduce the sensitivity characteristic gain below 4 kHz by expanding the control band, stabilizing the resonant modes. we set a gain margin of $g_{\rm m} = 5$ dB and a phase margin of $\phi_{\rm m} = 30$ deg as stability specifications.

C. Application to autonomous design method

From Sect. V-A, a $N_{\rm v} = 1$ stage notch filter is used to provide the velocity controller $C_{\rm v}(s)$ for stabilizing the resonance modes of the FSM. Therefore, the parameters $\boldsymbol{\rho}_{\rm SQP}$ and $\boldsymbol{\rho}_{\rm GA}$ designed using cooperative optimization can be defined as follows.

$$\boldsymbol{\rho}_{\rm SQP} = \begin{bmatrix} K_{\rm vp} & K_{\rm vi} \end{bmatrix} \in \mathbb{R}^{1\times 2} \tag{34}$$

$$\boldsymbol{\rho}_{\rm GA} = \begin{bmatrix} K_{\rm pp} & \zeta_{\rm vn1} & \zeta_{\rm vd1} & \omega_{\rm v1} & \omega_{\rm D} \end{bmatrix} \in \mathbb{R}^{1\times 5} \tag{35}$$

Table I shows the search range for (34) and (35). In this study, the search range is determined through the trial and error to obtain fine parameters. The same search range is set for parameter $\boldsymbol{\rho}$ in the GA-based autonomous design.

Subsequently, from Sect. V-B, the ideal sensitivity characteristic $S_{\rm ds}(s)$ is defined by the following equation, considering the proportional compensation of the position controller $C_{\rm p}(s)$ in the low frequency range, the integral compensation of the velocity controller $C_{\rm v}(s)$, and the steady-state gain characteristics of the FSM.

$$S_{\rm ds}(s) = \frac{k_{\rm ds}s}{s+\omega_{\rm ds}} \tag{36}$$

Here, the parameters in Table II were applied to $k_{\rm ds}$ and $\omega_{\rm ds}$ such that $S_{\rm ds}(s)$ satisfies a high-pass characteristic with the cutoff frequency of 4 kHz. The objective function $J_{\rm obj}(\boldsymbol{\rho}_{\rm SQP})$ was set to $N_{\rm obj} = 668$ frequencies logarithmically spaced between $\Omega_m^{\rm obj} = 2\pi \times \{100, \cdots, 4000\}$ rad/s.

Subsequently, considering the gain margin $g_{\rm m} = 5$ dB and phase margin $\phi_{\rm m} = 30$ deg, we formulated stability constraints for $\sigma_{\rm sm}$ and $r_{\rm sm}$ using the parameters in Table III. The angle a

TABLE I
PARAMETER SEARCH RANGE OF $\boldsymbol{\rho}_{\rm SQP}$ AND $\boldsymbol{\rho}_{\rm GA}$.

Parameter	Lower bound $\underline{*}$	Upper bound $\overline{*}$
$K_{\rm vp}$	0	1.0×10^{-5}
$K_{\rm vi}$	0	1.0×10
$K_{\rm pp}$	1.0×10^{3}	2.0×10^{6}
$\zeta_{\rm vn1}$	1.0×10^{-2}	1.2
$\zeta_{\rm vd1}$	1.0×10^{-1}	1.2
$\omega_{\rm v1}$ [rad/s]	$2\pi \times 5000$	$2\pi \times 20000$
$\omega_{\rm D}$ [rad/s]	$2\pi \times 500$	$2\pi \times 20000$

TABLE II
PARAMETERS OF THE DESIRED SENSITIVITY $S_{\rm ds}(s)$.

$k_{\rm ds}$	$\omega_{\rm ds}$ [rad/s]
1.0	$2\pi \times 4000$

TABLE III
PARAMETERS OF THE STABILITY CONSTRAINT.

$\sigma_{\rm sm}$	$r_{\rm sm}$	a	$W_{C\rm sm}$	$W_{l\rm sm}$
1.13	0.56	5	1.0×10^5	1.0×10^5

TABLE IV
SETTINGS OF GENETIC OPERATION.

Number of parameter optimization $N_{\rm para}$	200
Number of individuals $N_{\rm ind}$	10
Selection rate	1.00
Crossover rate	0.99
Mutation rate	0.08

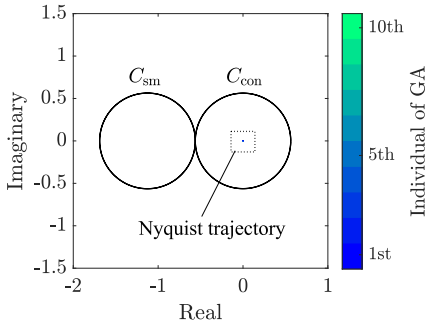

Fig. 6. Feasible Nyquist trajectories (reduced view).

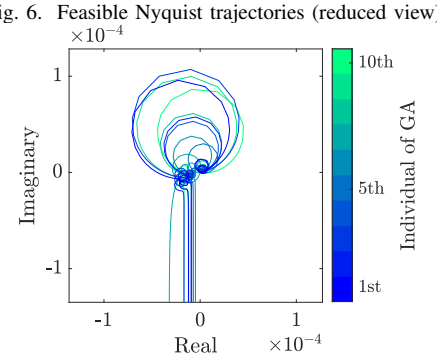

Fig. 7. Feasible Nyquist trajectories (magnified view).

of straight line $l_{\rm sm}$ and the weight values $W_{C\rm sm}$ and $W_{l\rm sm}$ are also shown in Table III. The stability constraint was imposed at $N_{\rm sm} = 1000$ frequencies logarithmically spaced between $\Omega_n^{\rm sm} = 2\pi \times \{100, \cdots, 25000\}$ rad/s. Note that $\Omega_m^{\rm obj}$ and $\Omega_n^{\rm sm}$ can be either logarithmically or linearly spaced.

Finally, κ in (30) was calculated as $\kappa = 6.6 \times 10^{-7}$, and $K_{\rm vi}^{\rm IP}$ is manually defined as $K_{\rm vi}^{\rm IP} := \kappa$. The initial point of SQP in the cooperative optimization method was set as $\boldsymbol{\rho}_{\rm SQP}^{\rm IP} = [0\ 6.6 \times 10^{-7}]$. Table IV shows the GA settings. The GA settings for the conventional GA-based method are the same as those in Table IV, but the number of generations $N_{\rm para}$ is set to $N_{\rm para} = 1000$. The FB controller design was performed on a computer (CPU: Intel® Xeon® Gold 6230, memory: 128 GB) using MATLAB®. We used the *fmincon* command from Optimization Toolbox™ for the SQP optimization, and our own program for the GA optimization.

D. Effect of the Proposed Initial Point Setting

To verify the effectiveness of the proposed initial point setting method, 10 sets of $\boldsymbol{\rho}_{\rm GA}$ within the range of Table I were randomly prepared, and the respective Nyquist trajectories at the initial point $\boldsymbol{\rho}_{\rm SQP}^{\rm IP}$ are shown in Fig. 6 and Fig. 7. From the figures, all Nyquist trajectories are described inside $C_{\rm con}$ and outside $C_{\rm sm}$. Therefore, $\boldsymbol{\rho}_{\rm SQP}^{\rm IP}$ successfully works as a feasible initial point regardless of any $\boldsymbol{\rho}_{\rm GA}$, as explained in Sect. IV-C.

E. Comparison of design efficiency

Fig. 8 shows the elite fitness values obtained by the cooperative optimization (CoOP) and the conventional GA-based (GA) methods. Both methods were implemented three times each.

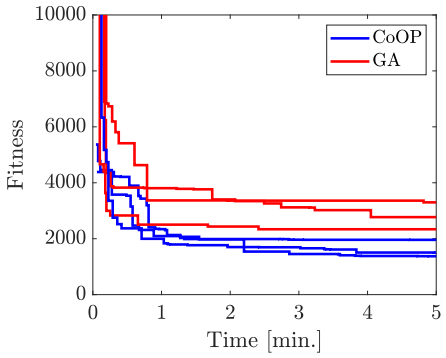

Fig. 8. Elite fitness values.

As shown in Fig. 8, the cooperative optimization method optimized the parameters more efficiently than the conventional GA-based method every time without getting optimization stuck. In particular, considering the final fitness, the average value obtained with the cooperative optimization method was 1613, which was 42 % lower than the average value of 2803 obtained with the conventional GA-based method.

F. Comparison of frequency characteristics

Table V lists the parameters designed using the cooperative optimization and the conventional GA-based methods. The table shows the best fitness values from the three tests for each method. From Table V, the gains of both the position and velocity controllers of the cooperative optimization method are larger than those of the conventional GA-based method. Fig. 9 shows the frequency characteristics of the integrated FB controller $C_{\rm all}(j\omega)(:= (C_{\rm p}(j\omega) + F_{\rm D}(j\omega))C_{\rm v}(j\omega))$. The cooperative optimization method yields a gain 1.45 dB higher than that of the conventional GA-based method below 1 kHz. As the main resonance mode at $2\pi \times 8540$ rad/s shown in Fig. 5 is in phase with -180 deg, the notch filter of the controller serves as a gain stabilizer. On the other hand, focusing on the high frequency region, band rejection properties are observed around the primary resonant mode in both methods. Figs. 10–12 show the open-loop characteristics, Nyquist plot, and sensitivity gain characteristics. In the open-loop characteristics shown in Fig. 10, the cooperative optimization method achieves a higher gain than that of the conventional GA-based method. The Nyquist plot shown in Fig. 11 satisfies the stability constraints specified by $C_{\rm sm}$ and $l_{\rm sm}$ while stabilizing the resonance modes. Finally, in the sensitivity gain characteristics shown in Fig. 12, the cooperative optimization method achieves a sensitivity 1.4 dB lower than that of the conventional method at 1 kHz or less. This indicates that effective optimization can be achieved, which confirms the effectiveness of the cooperative optimization method.

VI. Conclusion

In this paper, we adopted an autonomous design method based on a cooperative optimization combining SQP and GA for a position/velocity cascade FB control system. The

TABLE V
PARAMETERS OF THE FB CONTROLLER $C_{\rm p}(s)$, $C_{\rm v}(s)$, AND $F_{\rm D}(s)$.

Parameter	GA	CoOP
$K_{\rm vp}$	1.5×10^{-6}	2.2×10^{-6}
$K_{\rm vi}$	1.4×10^{-1}	1.5×10^{-1}
$K_{\rm pp}$	2.4×10^{5}	2.7×10^{5}
$\zeta_{\rm vn1}$	6.2×10^{-2}	5.1×10^{-2}
$\zeta_{\rm vd1}$	1.0	1.2
$\omega_{\rm v1}$ [rad/s]	$2\pi \times 7927$	$2\pi \times 7600$
$\omega_{\rm D}$ [rad/s]	$2\pi \times 4553$	$2\pi \times 17752$

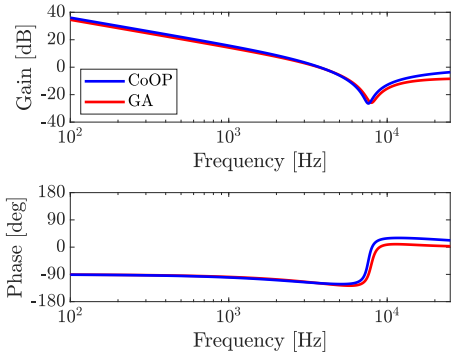

Fig. 9. FB controller $C_{\rm all}(j\omega)$.

cooperative optimization method can efficiently determine parameters that achieve low sensitivity while ensuring the desired stability margin without getting optimization stuck for the cascade control system. We confirmed the effectiveness of the cooperative optimization method by comparing it with the conventional GA-based method in an autonomous design problem for a laboratory FSM. As a future research topic, we would like to develop an autonomous design method with considering the robust stability against the plant perturbation.

ACKNOWLEDGMENT

This work was supported by The Nitto Foundation, Japan.

REFERENCES

[1] Z. Z. Liu, F. L. Luo, and M. A. Rahman, "Robust and precision motion control system of linear-motor direct drive for high-speed $X-Y$ table positioning mechanism," *IEEE Trans. Ind. Electron.*, vol. 52, no. 5, pp. 1357–1363, 2005.

[2] P. Lin, Z. Wu, Z. Fei, and X.-M. Sun, "A generalized PID interpretation for high-order LADRC and cascade LADRC for servo systems," *IEEE Trans. Ind. Electron.*, vol. 69, no. 5, pp. 5207–5214, 2022.

[3] Y. Maeda and M. Iwasaki, "Circle condition-based feedback compensation with frequency shaping for improvement of settling performance," *IEEE Trans. Ind. Electron.*, vol. 61, no. 10, pp. 5500–5508, 2014.

[4] Y. Maeda, S. Kunitate, E. Kuroda, and M. Iwasaki, "Autonomous cascade structure feedback controller design with genetic algorithm-based structure optimization," in *Proc. 21st IFAC World Congr.*, pp. 8529–8535, 2020.

[5] H. Wu, W. Su, and Z. Liu, "PID controllers: design and tuning methods," in *Proc. 9th IEEE Conf. Ind. Electron. Appl.*, pp. 808–813, 2014.

[6] R. Kitayoshi and H. Fujimoto, "Automatic adjustment method of controller structure and parameter based on structured $\rm H_\infty$ control," in *Proc. 45th Annu. Conf. IEEE Ind. Electron. Soc.*, pp. 3263–3268, 2019.

[7] P. Apkarian and D. Noll, "Nonsmooth $\rm H_\infty$ synthesis," *IEEE Trans. Autom. Control*, vol. 51, no. 1, pp. 71–86, 2006.

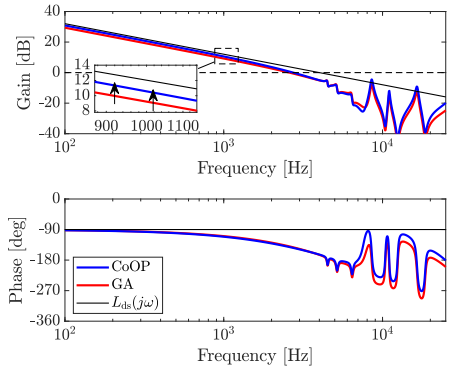

Fig. 10. Open-loop characteristics $L(j\omega)$.

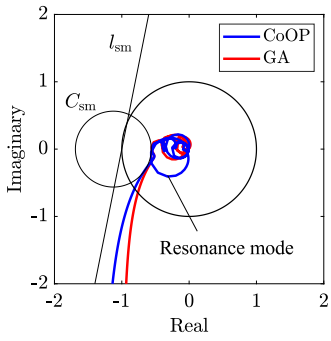

Fig. 11. Nyquist diagram of $L(j\omega)$.

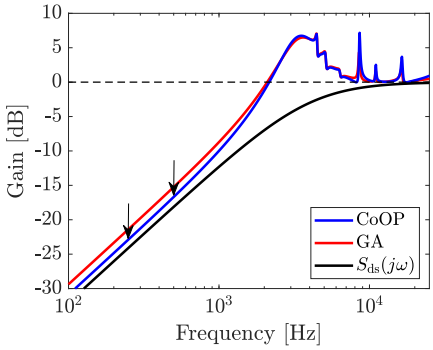

Fig. 12. Sensitivity characteristics $S(j\omega)$.

[8] Y. Hui, Z. Yan, W. Z. Long, and Y. Chao, "Adaptive double-loop PID control method of DC motor based on the GA-FNC algorithm," in *Proc. 2012 8th IEEE Int. Symp. Instrum. Control Technol.*, pp. 324–329, 2012.

[9] T. R. Biyanto, M. S. Alfarisi, N. Afdanny, H. Setiawan, and A. Hasan, "Simultaneous optimization of tuning PID cascade control system using duelist algorithms," in *Proc. 2016 Int. Seminar Intell. Technol. Appl.*, pp. 601–606, 2016.

[10] C. Guo, Q. Song, and W. Cai, "A neural network assisted cascade control system for air handling unit," *IEEE Trans. Ind. Electron.*, vol. 54, no. 1, pp. 620–628, 2007.

[11] Y. Maeda, E. Kuroda, T. Uchizono, and M. Iwasaki, "Hybrid optimization method for high-performance cascade structure feedback controller design," in *Proc. 44th Annu. Conf. IEEE Ind. Electron. Soc.*, pp. 4588–4593, 2018.

[12] E. Kuroda, Y. Maeda, and M. Iwasaki, "Autonomous parameter design for cascade-structure feedback controller based on cooperative optimization method," *IEEJ J. Ind. Appl.*, vol. 10, no. 4, pp. 457–468, 2021.